Theta activity paradoxically boosts gamma and ripple frequency sensitivity in prefrontal interneurons

Ricardo Martins Merino^{a,b,c,d,e}, Carolina Leon-Pinzon^{a,b,c,e}, Walter Stühmer^{c,e}, Martin Möck^f, Jochen F. Staiger^f, Fred Wolf^{a,b,c,e,g,h}, and Andreas Neef^{a,b,c,e,g,h,1}

^aMax Planck Institute for Dynamics and Self-Organization, Göttingen 37077, Germany; ^bGöttingen Campus Institute for Dynamics of Biological Networks, University of Göttingen, Göttingen 37073, Germany; Gernstein Center for Computational Neuroscience, Göttingen 37073, Germany; Göttingen Graduate Center for Neurosciences, Biophysics, and Molecular Biosciences, University of Göttingen, Göttingen 37077, Germany; *Max Planck Institute of Experimental Medicine, Göttingen 37075, Germany; finstitute for Neuroanatomy, University Medical Center Göttingen, University of Göttingen, Göttingen, Göttingen 37075, Germany; ⁹Institute for the Dynamics of Complex Systems, University of Göttingen, Göttingen 37077, Germany; and ^hCenter for Biostructural Imaging of Neurodegeneration, University Medical Center Göttingen, University of Göttingen, Göttingen 37075, Germany

Edited by György Buzsáki, Neuroscience Institute, New York University Grossman School of Medicine, New York, NY; received August 6, 2021; accepted November 7, 2021

Fast oscillations in cortical circuits critically depend on GABAergic interneurons. Which interneuron types and populations can drive different cortical rhythms, however, remains unresolved and may depend on brain state. Here, we measured the sensitivity of different GABAergic interneurons in prefrontal cortex under conditions mimicking distinct brain states. While fast-spiking neurons always exhibited a wide bandwidth of around 400 Hz, the response properties of spike-frequency adapting interneurons switched with the background input's statistics. Slowly fluctuating background activity, as typical for sleep or quiet wakefulness, dramatically boosted the neurons' sensitivity to gamma and ripple frequencies. We developed a time-resolved dynamic gain analysis and revealed rapid sensitivity modulations that enable neurons to periodically boost gamma oscillations and ripples during specific phases of ongoing low-frequency oscillations. This mechanism predicts these prefrontal interneurons to be exquisitely sensitive to highfrequency ripples, especially during brain states characterized by slow rhythms, and to contribute substantially to theta-gamma cross-frequency coupling.

cross-frequency coupling | dynamic gain | interneuron | information

Collective rhythmic activity is implicated in brain functions from sensory information processing to memory consolidation, often with higher-frequency activity bouts locked onto lower frequencies (1-3). While the mechanism behind this cross-frequency coupling is unclear (3), the initiation and maintenance of gamma band (30 to 150 Hz) oscillations are closely associated with fast-spiking (FS) parvalbumin-positive interneurons (4, 5). When driven with frequency chirps, and as a result of intrinsic membrane properties, FS neurons fire more robustly at higher input frequencies than spike-frequency adapting (AD) somatostatin-positive interneurons, which are most responsive to lower frequencies (6). Nevertheless, recent studies strongly suggest that, under certain conditions, somatostatinpositive interneurons are crucial for gamma oscillations (7-9). Could the spectral sensitivity of different interneuron populations perhaps be itself state dependent? Here, we characterized cortical GABAergic interneurons at different in vivo-like working points by measuring their dynamic gain (10–14).

Dynamic gain quantifies how input in different frequency bands modulates population firing under in vivo-like conditions of fluctuating background input. To probe the potential impact of different brain states on spectral sensitivity, we used different types of background inputs that mimic the strength and timescales of correlations in background input across brain states (15). We find that both FS and AD interneuron populations can have remarkably wide bandwidths (up to about 500 Hz),

making them capable of tracking fast input frequencies well into the range of sharp wave ripples.

Moreover, our results uncover unanticipated flexibility in AD neurons, which can massively shift their frequency preference, specifically engaging or disengaging with high-frequency rhythms, such as gamma and sharp wave ripples. The presence or absence of slowly correlated input drives this sensitivity shift, which can occur within 50 ms, in phase with an ongoing slow rhythm. This observation offers a mechanistic explanation for theta-gamma cross-frequency coupling.

Results

AD and FS (Fig. 1 A and B) are the most common firing patterns of somatostatin- and parvalbumin-positive interneurons, respectively (16). Their spectral selectivity has been investigated through subthreshold and suprathreshold cellular responses to simple, purely sinusoidal inputs (6) (Fig. 1 C and D). However, in vivo, even when activity on the population level is periodic, the firing of individual neurons appears stochastic, driven by noisy, fluctuating inputs rather than pure sinusoids (13, 17). We thus probed the spectral sensitivity of mouse layer 2/3

Significance

Rhythmic brain activity is a signature of information processing. Common inhibitory cells, spike-frequency adapting interneurons, are typically thought to only participate in low-frequency rhythms (<10 Hz). However, we found that these cells' frequency preference can be switched from 2 to 200 Hz. The switch occurs when low-frequency components dominate the interneurons' input, as is the case during brain states of slowwave sleep or quiet rest. These interneurons not only increase their sensitivity to input in the 30 to 200 Hz range (gamma and ripples) they do so within a few dozen milliseconds, in phase with the low-frequency input components. Our findings reveal unexpected flexibility in neurons, which could shape thetagamma cross-frequency coupling, a phenomenon thought to contribute to information routing.

Author contributions: R.M.M., W.S., J.F.S., F.W., and A.N. designed research; R.M.M., C.L.-P., and M.M. performed research; R.M.M. and A.N. analyzed data; and R.M.M., F.W., and A.N. wrote the paper.

The authors declare no competing interest.

This article is a PNAS Direct Submission.

Published under the PNAS license.

¹To whom correspondence may be addressed. Email: aneef@gwdg.de.

This article contains supporting information online at http://www.pnas.org/lookup/ suppl/doi:10.1073/pnas.2114549118/-/DCSupplemental.

PNAS 2021 Vol. 118 No. 51 e2114549118

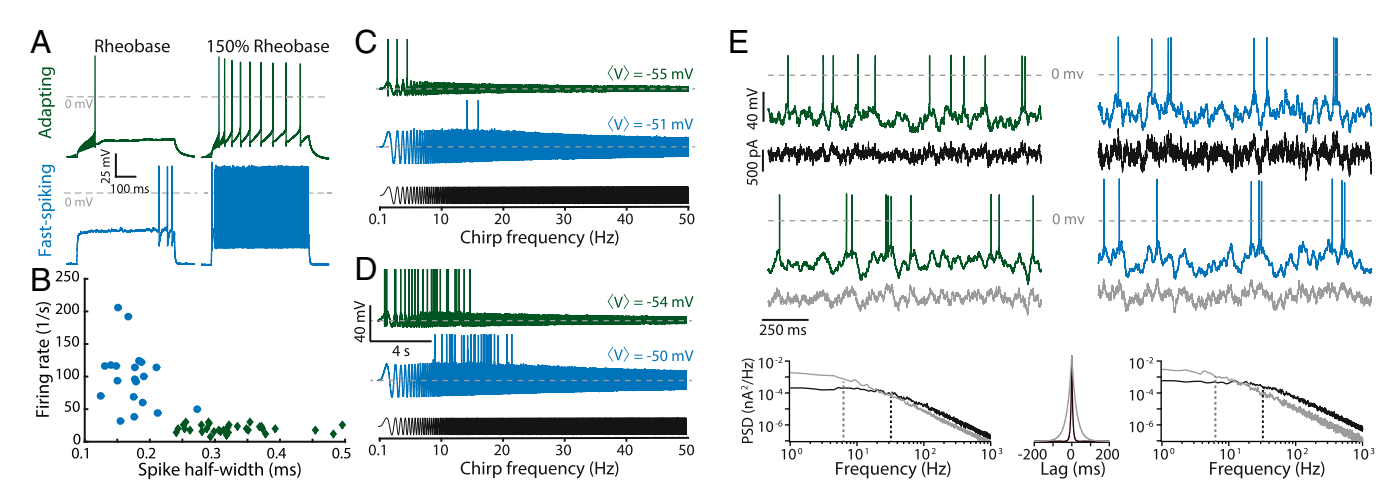


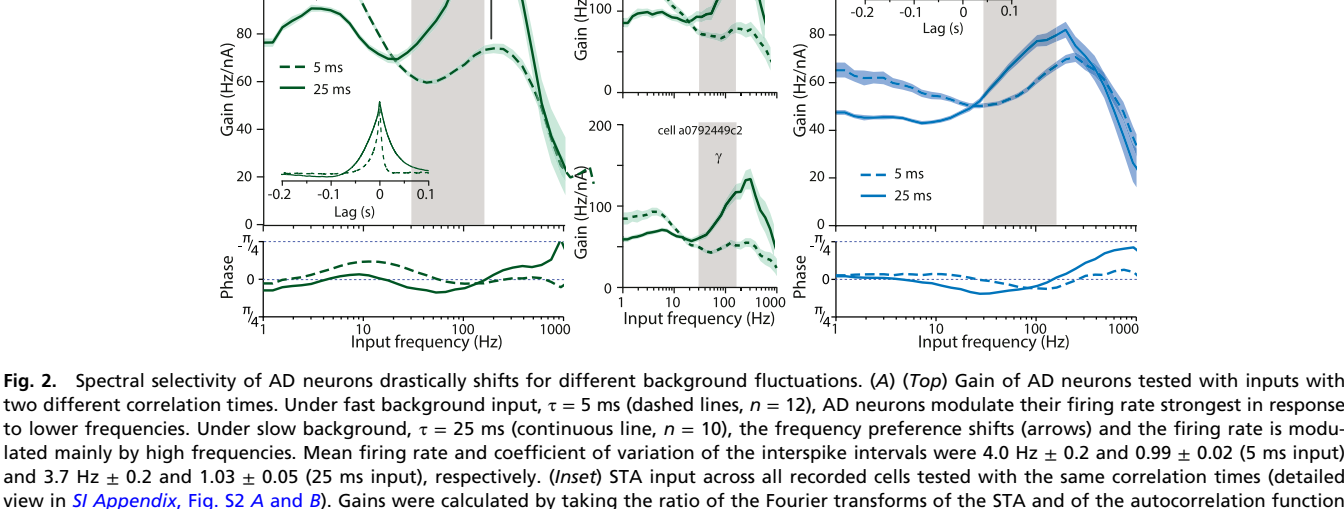
Fig. 1. Characterization of neocortical adapting and FS interneurons. (A) Square pulses of 500 ms were used to determine the recorded neuron's firing pattern at the 150% rheobase level. Shown are representative responses of AD (green) and FS (blue) neurons at rheobase and 150% rheobase. (B) Spike half-width and firing rate allow a clear distinction between these cell types. (C) Frequency chirp currents (black) have been used to characterize the spectral sensitivity of neurons. They yield APs (shown clipped) at lower input frequencies for AD neurons than for FS neurons. (D) A slight increase in the offset current, resulting in only a 1 mV depolarization, already results in overlapping bandwidths for AD and FS neurons. This strong dependence of the "preferred frequency" on the baseline voltage indicates substantial uncertainty in chirp-based characterizations. (E) We assessed neuronal encoding performance in two in vivo-like regimes, distinguished by the correlation time of the fluctuating stimuli (τ = 5 ms, black, and τ = 25 ms, gray). The stimulus amplitude at each trial was adjusted to achieve a target operating point (characterized by firing rate and spike train irregularity; see Materials and Methods). The corresponding voltage traces of AD and FS neurons are shown above the stimuli, and the power spectral densities (PSDs) and autocorrelations of the inputs are shown at the bottom. The dashed lines in the PSDs indicate the cutoff frequencies (32 and 6.4 Hz) corresponding to the correlation times of the different inputs.

prefrontal FS and AD interneuron populations under naturalistic operating conditions (Fig. 1*E*). These dynamic gain measurements require precise control over the neurons' input to a degree that cannot be attained in vivo. We therefore used patch-clamp recordings in current-clamp mode in acute prefrontal slices to establish two different regimes of fluctuating input, distinguished by the correlation time τ : the first case, $\tau = 5$ ms, mimics the case of completely asynchronous population activity, when the decay time constant of synaptic currents is the only source of input correlations (Fig. 1*E*, black traces). The other input, characterized by a much slower 25 ms correlation time, i.e., a cutoff frequency in the range of theta frequencies, mimics brain states with population activity exhibiting slow fluctuations, such as quiet wakefulness or slow-wave sleep (15) (Fig. 1*E*, gray traces).

Input Correlations Determine Frequency Selectivity. The spectral sensitivity of interneurons was markedly different from their chirp responses, and for AD cells, it changed drastically between the two conditions (Fig. 2A). In the asynchronous regime, AD neurons respond preferentially to slow components, with the highest sensitivity in the 2 to 4 Hz range (mean dynamic gain = 119 Hz/nA, 95% bootstrap CI: [117, 122]). The average gain in the gamma range (Fig. 2A, shaded region) reaches only 62% of the average at lower frequencies (<20 Hz) (64 Hz/nA [63, 65] vs. 103 Hz/nA [101, 105]). As detailed in the Materials and Methods and SI Appendix, Fig. S1, these values mean that the addition of a small, 10 pA sinusoidal modulation (equivalent in magnitude to a single synaptic event) on top of the irregularly fluctuating background input would modulate the AD population's firing rate by 1.2 Hz in response to a superimposed 3 Hz input, but it would modulate the firing rate only by 0.6 for 60 Hz, indicating a clear preference for lower frequencies. This preference, however, changed completely when AD neurons were exposed to slowly fluctuating input such that their preferred frequency shifted from 2 to 200 Hz. The gain at 2 to 4 Hz dropped from 119 Hz/nA [117, 122] to 91 Hz/nA [89, 92], and the gain at 200 Hz increased from 74 Hz/nA [72, 76] to

119 Hz/nA [113, 124]. Fig. 2B demonstrates the occurrence of this shift in two individual AD neurons. With this abrupt change in frequency preference, AD neurons in the synchronous regime become more sensitive to gamma input than to lower frequencies (average gains: 97 Hz/nA [94, 101] vs. 81 Hz/nA [80, 83]). Altogether, these data reveal that, during network states characterized by slow background fluctuations, AD cells tune themselves to gamma and higher-frequency input. FS interneurons, on the other hand, preferentially transmit high frequencies irrespective of the input correlations, with a maximum sensitivity around 200 to 250 Hz (Fig. 2C). Both FS interneurons and, given sufficiently slow input components, AD interneurons have a remarkably wide bandwidth, with a high-frequency limit well above 400 Hz, an order of magnitude higher than expected from their chirp responses. The particularly strong change in AD neurons' frequency preference led us to hypothesize that changes in specific low-frequency bands might substantially improve high-frequency encoding.

Theta Input Reliably Boosts Gamma and Ripple Sensitivity of AD **Neurons.** This input-dependent spectral sensitivity might allow AD neurons to provide brain state-dependent feedback input into the local cortical circuit. Interestingly, AD neurons shift their preference to the gamma band when lower frequencies dominate their input. This suggests that the presence of theta oscillations (4 to 12 Hz) could tune them to higher frequencies, boosting gamma components. To test this hypothesis, we exposed AD neurons to the rapidly fluctuating 5 ms correlated background input, either on its own or supplemented with theta-band components (Fig. 3A). This addition increased the power in the 4 to 12 Hz band from 15% of the total power to 45%. We chose this amount of theta-band addition because the resulting power spectra resemble those of LFPs from the prefrontal cortex of mice at rest (18). Simply adding input components would have increased the AD neurons' firing rate. Instead, we scaled the input fluctuations to 70% to keep the firing rates constant and thereby warrant an unbiased comparison of encoding capability (Fig. 3A). We found that the theta-band



C₁₂₀

100

two different correlation times. Under fast background input, $\tau = 5$ ms (dashed lines, n = 12), AD neurons modulate their firing rate strongest in response to lower frequencies. Under slow background, $\tau = 25$ ms (continuous line, n = 10), the frequency preference shifts (arrows) and the firing rate is modulated mainly by high frequencies. Mean firing rate and coefficient of variation of the interspike intervals were 4.0 Hz \pm 0.2 and 0.99 \pm 0.02 (5 ms input) and 3.7 Hz \pm 0.2 and 1.03 \pm 0.05 (25 ms input), respectively. (Inset) STA input across all recorded cells tested with the same correlation times (detailed view in SI Appendix, Fig. S2 A and B). Gains were calculated by taking the ratio of the Fourier transforms of the STA and of the autocorrelation function of the input (shown in SI Appendix, Fig. S2 C and D). Gray columns represent the gamma frequency band, and the shaded region around gain curves represents the 95% bootstrap CI. (Bottom) Phase of firing rate modulation with respect to input. No substantial phase delays are associated with AP generation. (B) Individual gain curves of two AD cells from A for both correlation times. The drastic shift in frequency preference is clearly visible at the singlecell level. (C) As in A, but for FS neurons. Those display a wide bandwidth and no drastic shifts in frequency preference ($\tau = 5$ ms, dashed lines, n = 7; τ = 25 ms, continuous lines, n = 9). Grand-averaged firing rate and coefficient of variation of the interspike intervals were 5.0 Hz \pm 0.6 and 1.12 \pm 0.24 (5 ms) and 3.6 Hz \pm 0.2 and 1.47 \pm 0.10 (25 ms). Numbers are given as mean \pm SEM.

 B_{200}

components indeed boosted the gain for frequencies above 30 Hz, with the average gamma band gain increasing from 71 Hz/nA [69, 73] to 86 Hz/nA [83, 89] and the average gain in the ripple band increasing from 79 Hz/nA [77, 82] to 105 Hz/ nA [101, 110] (Fig. 3B). The gamma/theta ratio increased in 9 out of 10 cells, from 0.56 ± 0.02 to 0.74 ± 0.05 , while the ripple/ theta ratio increased from 0.63 ± 0.02 to 0.88 ± 0.05 (mean \pm SEM; Fig. 3C), revealing that, indeed, an increase in theta power boosts gamma and ripple sensitivity of AD neurons.

100

Theta Phase Determines Gamma Sensitivity. The aforementioned dynamic gain curves are based on the timing of all action potentials (APs) fired during a long stimulus period. They represent the average frequency selectivity for given input statistics and allowed us to detect the boosting for gamma and ripple frequencies during 30-s-long periods of theta-dominated input. During in vivo activity, however, short gamma bursts or ripples occur phase-locked to slower rhythms, consistent with the idea that neurons might be recruited to high-frequency rhythms within a few dozen milliseconds. Specifically, theta-gamma cross-frequency coupling suggests a modulation of gamma sensitivity throughout the phase of the ongoing theta rhythm. To test whether AD neurons indeed display such a modulation, we developed a time-resolved decomposition of the dynamic gain. Reanalyzing the data obtained with the theta-supplemented stimulus (Fig. 3), we determined the phase φ_{θ} of the stimulus theta band at each AP time. We sorted the APs into three groups, according to φ_{θ} . The boundaries between groups, φ_{θ} = -0.017 and $\varphi_{\theta} = 0.476$, were chosen so that each group contained one-third of all APs (Fig. 4 A and B and Materials and Methods). For each group, the average gain across all 10 neurons was determined as before (Fig. 4C). As expected for a meaningful decomposition, the three gain components combined to replicate the overall dynamic gain (Inset in Fig. 4C). For each neuron, we calculated three dynamic gain curves, each derived from all the APs belonging to one φ_{θ} group. The neuron's ability to lock to gamma rhythms was quantified as the average gain value in the gamma range (30 to 150 Hz). Across

the 10 neurons, the median value of this gamma sensitivity increased from 27.4 to 37.5 Hz/nA as φ_{θ} goes from the first to the third group, revealing a theta-phase dependent locking of APs to gamma inputs (Fig. 4D). The substantially increased gamma sensitivity for APs fired later during a theta cycle indicates that AD neurons' frequency tuning changes within a quarter of a theta cycle, i.e., within less than 50 ms.

NEUROSCIENCE

This decomposition of the dynamic gain curve, by grouping of APs according to the theta phase, is applicable to any dataset as long as the theta band has substantial power. For an Ornstein-Uhlenbeck process with a correlation time of 25 ms, about 30% of the overall power occurs in the theta band. We analyzed the 25 ms datasets for AD and FS neurons (Fig. 2) in this way. While the AD neurons showed a similarly strong variation of the gamma sensitivity during the theta cycle also for these different input statistics, the theta-phase dependency of FS neurons' high-frequency encoding was much smaller (SI Appendix, Fig. S4).

Discussion

Our study reveals a surprising type of dynamic regulation of AD neuron's response properties. When the neurons' input fluctuates rapidly, as during active wakefulness, our data support the traditional picture in which AD neurons preferentially encode low-frequency input and FS neurons encode highfrequency (>30 Hz) input. A drastic change in the frequency preference of AD neurons occurs, however, when input correlations are slow, as during brain states featuring low-frequency dominated local field potentials. Under such conditions, AD neurons react preferentially to gamma and ripple frequencies. Our findings thus uncover an unanticipated flexibility of interneuron function that allows brain states to tune AD neuron population coding and might underlie their reported contribution to gamma oscillations (7, 9).

Previously, dynamic gain curves were studied as essentially static properties, determined from minute-long stimuli of stationary stochastic properties. Our time-resolved analysis revealed that AD neurons rapidly respond to fluctuations in

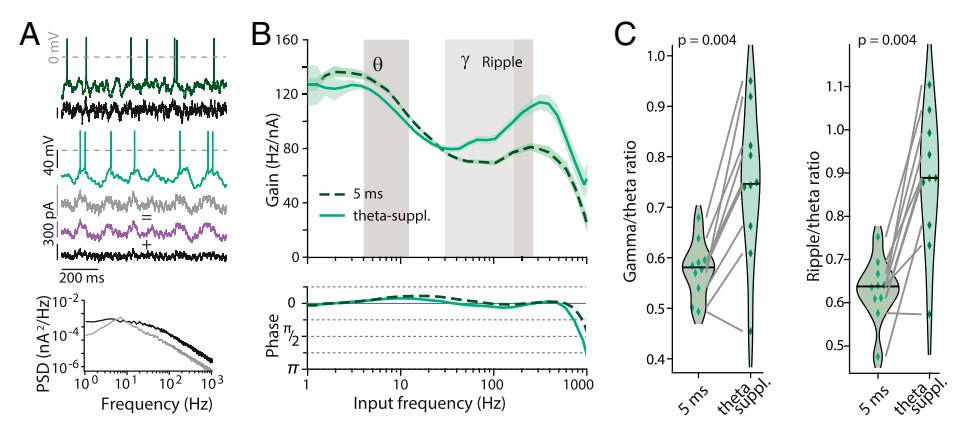


Fig. 3. Increasing theta input to AD neurons boosts sensitivity to gamma and ripple frequencies. (A) Sample stimuli and voltage traces (dark green, 5 ms input; light green, theta-supplemented input) and power spectral density of noisy inputs with $\tau = 5$ ms (black) and theta-supplemented 5 ms input (gray). Theta-supplemented input was constructed by adding a theta bandpass filtered white noise input (purple) to the 5 ms input. Overall signal power was adjusted to achieve 5 Hz firing; this required a reduction to 70 ± 4%. Grand-averaged firing rate and coefficient of variation of the interspike intervals were 4.58 Hz \pm 0.23 and 0.97 \pm 0.03 (5 ms input) and 4.78 Hz \pm 0.26 and 0.92 \pm 0.04 (theta-supplemented 5 ms input). (B) (Top) Gain of AD cells tested with both $\tau = 5$ ms (dashed line) and theta-supplemented 5 ms (continuous line) inputs (n = 10). Boosting theta in the input paradoxically reduces the sensitivity of AD neurons to this frequency band while promoting sensitivity to gamma and ripple frequencies (150 to 250 Hz). (Bottom) The phase of firing rate modulation with respect to the input. No substantial phase delays are associated with AP generation, even though the gain magnitude is modulated. (C) Ratios between average gains at gamma and theta (Left) and ripple and theta (Right) for the individual neurons (diamonds). Both ratios increase when theta power in the input is increased. Gamma/theta ratio for $\tau = 5$ ms: 0.56 ± 0.02 vs. theta-supplemented 5 ms: 0.74 ± 0.05 , n = 10 (paired sample, two-sided Wilcoxon signed-rank test, W = 1, P = 0.004). Ripple/theta ratio for $\tau = 5$ ms: 0.63 ± 0.02 vs. theta-supplemented 5 ms: 0.88 ± 0.05 , n=10 (two-sided Wilcoxon signed-rank test, W = 0, P=0.002). Violin plots show the medians as bars. Numbers are given as mean \pm SEM.

input statistics, increasing their dynamic gain in the gamma band by 50% within a few dozen milliseconds. Our decomposition approach provides a powerful extension to current population encoding analyses. It allows, for instance, a quantitative comparison between the encoding capacity of APs within ripples versus outside ripples or of AP duplets as compared to isolated APs.

Increased encoding of high frequencies (>30 Hz) during particular phases of strong, slow (theta) components (Figs. 3 and 4) closely matches the phenomenon of theta-gamma crossfrequency coupling (19). In the dynamics of recurrent local circuits, the dynamic gain is a main component to the feedback gain that determines whether a collective oscillation is amplified or dies out. In theoretical studies of population oscillations in synchronous (2) or asynchronous (20) network states, the magnitude and the phase of the dynamic gain are key determinants of oscillation strength and frequency (21). Therefore, the small phase delays associated with AP generation (Figs. 2 A and C and 3B) and the input-dependent increase in gain magnitude predict a boost of gamma oscillation amplitude in the presence of theta-frequency input components and in particular during late theta-phases. The dynamic tuning of spectral sensitivity in phase with slow input fluctuations offers a long-sought mechanism coupling gamma amplitude to theta oscillations that is based on cellular electrophysiological properties.

The wide bandwidth of AD and FS neurons of up to 500 Hz and a maximal sensitivity reached around 200 Hz is by itself a striking phenomenon. In cortical pyramidal neurons, high bandwidth dynamic gain is known to mediate the submillisecond precision of population coding for input changes (22), but what function could a narrow preference band at around 200 Hz serve? Retrieval and consolidation of episodic memory require a complex and precise replay of activity by cell assemblies in the form of high-frequency sharp wave ripples (150 to 250 Hz). Intriguingly, these occur specifically during periods of synchronous network activity, such as during slow-wave sleep or quiet wakefulness (23), when, as we showed, AD and FS neurons are most sensitive to high frequencies. Given the input-dependent selectivity switch in AD neurons, slow oscillations may, in genboost high-frequency sensitivity of interneurons and eral.

specifically allow AD neurons to tune in to ripple-related inputs and disinhibit cortical circuits in a precisely timed manner.

Can we expect to find theta-phase dependent gamma sensitivity in vivo? The dynamic gain curve of neurons in vivo was determined once and found to be similar to measurements in cortical slices (22). However, the frequency sensitivity in AD neurons strongly depends on the input's spectral composition. The lack of precise voltage-clamp measurements of input currents in vivo prevents a direct comparison. Nevertheless, we can compare the input currents' power spectrum to the spectrum of local field potentials recorded in mice. In both signals, 30 to 50% of the total power occurs in the theta band, and the peak occurs around 5.5 Hz (18). However, in the in vivo signals, the power is even more focused on a narrower band within the theta region. The firing rate modulation caused by this theta component in AD neurons ex vivo is reported in Fig. 4B and SI Appendix, Fig. S3B. Modulation in vivo for non-fast-spiking, hippocampal interneurons during hippocampal theta oscillations (24) is somewhat less pronounced than in SI Appendix, Fig. S3B but not substantially different. These parallels suggest that inputs in vivo could be expected to cause AD neurons to display a behavior that is quantitatively similar to the one reported here.

A mechanistic understanding of the reported phenomena and their relevance for in vivo information processing requires a combination of approaches. More relevant current inputs for ex vivo dynamic gain measurements could be designed by matching the statistics of membrane potential fluctuations to those observed in vivo. Network models with neurons displaying theta-dependent encoding could reveal the relation of single neuron frequency sensitivity and the occurrence of network gamma. Oscillations in recurrent networks depend critically on synaptic strength and delays. Their contributions might explain why gamma oscillations in vivo peak slightly earlier (25) than our findings for AD neuron suggest. Finally, spectrally resolved sensitivity measurements in vivo (22, 26) could be used to investigate brain state-dependent sensitivity changes.

Materials and Methods

Animals and Slice Preparation. All experiments were performed in accordance with institutional and state regulations (Niedersächsisches Landesamt für

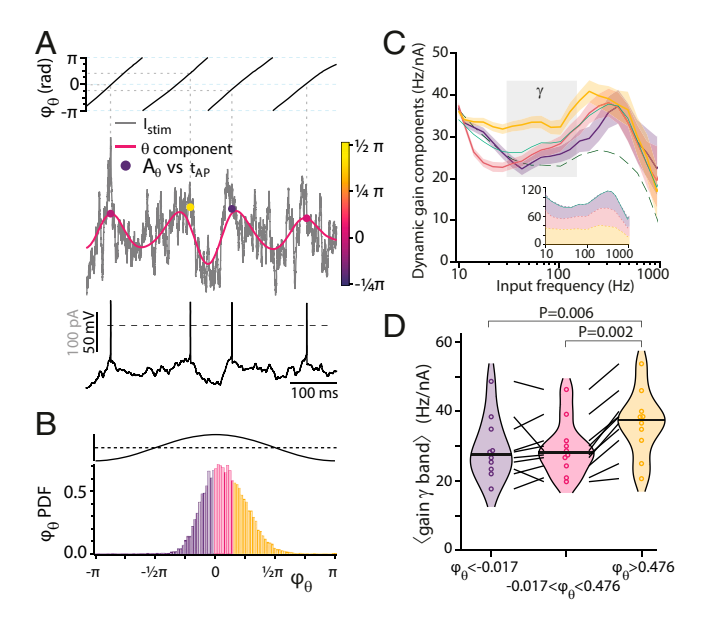


Fig. 4. Sensitivity to gamma frequencies is modulated during progression through the theta cycle. (A) Analysis of theta components showing the membrane voltage (bottom, black), input current (gray), its theta component (magenta; see Materials and Methods), and points indicating the time of APs, plotted against the instantaneous theta amplitude $\boldsymbol{A}_{\boldsymbol{\theta}}$ obtained by Hilbert analysis. The color code corresponds to the theta phase (ϕ_{θ}, Top) . (B) A probability density plot of ϕ_{θ} with three differently colored phase intervals. Each interval contains one-third of all APs. The top trace indicates the cosine relation between the theta component's phase and amplitude. (C) The dynamic gain curves of the three components (color code as in B) have distinctive frequency dependencies. Their 95% CIs (shaded) separate in the beta (12 to 30 Hz) and gamma frequency bands. For reference, the two dynamic gain curves from Fig. 3B are added. scaled by one-third to account for different amplitudes due to the trisection of the curves. The comparison reveals that the gamma band encoding of the earliest group is as poor as encoding without theta supplement. The latest group, however, displays much better gamma encoding than the average. In the inset, the three components are stacked. Their sum closely reproduces the overall dynamic gain obtained with the thetasupplemented input from Fig. 3B (replotted in green). (D) AD neurons' sensitivity to gamma frequencies (Materials and Methods) increases during the theta cycle from the lower two ϕ_{θ} intervals, 29.4 \pm 2.9 Hz/nA (purple, Left) and 29.4 \pm 2.6 Hz/nA (magenta, center), to the APs with the highest φ_{θ} values, 36.5 \pm 3.0 Hz/nA (orange, Right). Gamma sensitivity in the latest interval (orange) is significantly higher than in the first (purple, W=2, P=0.006) and the second (magenta, W=0, P=0.002) based on paired sample, two-sided Wilcoxon signed-rank tests.

Verbraucherschutz und Lebensmittelsicherheit). Experiments were performed in 3 to 8-wk-old mice of either sex from five different mouse lines. Two lines target mostly AD interneurons: GIN [FVB-Tg(GadGFP)45704Swn, The Jackson Laboratory #003718] and SOMCrexAi9 [Ssttm2.1(cre)Zjh/J, The Jackson Laboratory #013044, crossbred with B6.Cg-GT(ROSA)26Sor^tm9(CAG-tdTomato)Hze/ J, The Jackson Laboratory #007909]; and three lines target mostly FS interneurons: PVCre (27), PVCrexAi32 [PVCre crossbred with B6;129S-Gt(ROSA)26-Sortm32(CAG-COP4*H134R/EYFP)Hze/J, The Jackson Laboratory # 012569], and Nkx2.1CreERxAi14 [Nkx2-1tm1.1(cre/ERT2)Zjh/J, The Jackson Laboratory # 014552, crossbred with B6;129S6-Gt(ROSA)26Sortm14(CAG-tdTomato)Hze/J, The Jackson Laboratory # 007908]. Animals were kept in standard 12 h light regime with water and food ad libitum. Animals were intraperitoneally injected with a mixture of ketamine and xylazine in phosphate-buffered saline (respectively 100 and 20 mg/kg of body weight) and decapitated. The brain was quickly removed and kept in ice-cold, carbogen-saturated cutting solution containing, in millimolars, 125 NaCl, 2.5 KCl, 26 NaHCO₃, 1.25 NaH₂PO₄, 0.4 ascorbic acid, 4 Na-lactate, 25 glucose, 1 MgCl₂, and 2 CaCl₂ (~315 mOsm, pH 7.4). The 300- μ m-thick coronal neocortical slices were made in a VT1200S Vibratome (Leica) and incubated at 35 °C in carbogen-saturated recording solution (artificial cerebrospinal fluid [aCSF], in millimolars: 125 NaCl, 4 KCl, 26 NaHCO₃, 10 glucose, 1.3 MgCl₂, and 2 CaCl₂) until recorded.

Patch-clamp Recordings. One slice at a time was transferred to a heated recording chamber (PH6 and RC-27L, Warner Instruments) and mechanically stabilized with a slice hold-down (SHD-27LH/15, Warner Instruments). Throughout the experiment, the slice was gravitationally perfused with warm aCSF through an in-line heater (HPT-2, Alasciences) at a 1 to 2.5 mL/min flow rate. Both the recording chamber and the in-line heater were controlled by a TC-20 temperature controller (NPI Electronic). Temperature settings were adjusted so that a thermistor measured a target temperature of 36 \pm 1 °C at the slice position. Slices were visualized in an Axio Examiner.D1 microscope (Zeiss) equipped with a W Plan-Apochromat 40×/1.0 DIC objective. Cells were visualized with infrared differential interference contrast optics (Zeiss), and fluorescent signal was imaged with a multiwavelength light source (pE-4000, CoolLed) and a charge-coupled device camera (MD061RU-SY, Ximea). Four to six MOhm pipettes were prepared from borosilicate glass capillaries (PG10165-4, World Precision Instruments) in a vertical puller (PIP 6, HEKA). Internal solution contained, in millimolars, 135 K-gluconate, 10 KCl, 4 NaCl, 0.1 Na₄EGTA, 1 Mg-ATP, 0.3 Na-GTP, 10 Hepes, 0.5 $\mathrm{Na_2}$ -phosphocreatine, and 0.2% (wt/vol) biocytin (285 to 290 mOsm, pH adjusted to 7.3). Whole-cell current-clamp recordings were made in an EPC-10 double amplifier controlled by Patchmaster (Heka). Fast and slow capacitances and series resistance were carefully adjusted in voltage-clamp mode before recording; fast capacitances while in on-cell configuration, and slow capacitances after achieving whole-cell configuration. Series resistance was 90 to 100% compensated with a feedback time constant of 10 µs. Voltage signals were low-pass filtered at 8.8 kHz and digitized at 100 kHz. Data analyses were performed in custom-written Matlab 2014b (Mathworks) and Igor Pro-8 and 9 (Wavemetrics) programs. Liquid junction potential of -14 mV was not corrected. All experiments were performed in the presence of blockers of GABA receptors (picrotoxin, 30 µM, Sigma) and glutamate receptors (NBQX, 10 μM, Tocris, and DL-AP5, 30 μM, Sigma).

Characterization of AP Firing Patterns. Layer 2/3 interneurons were identified via fluorescence imaging. In order to identify their electrical type, 500-ms-long current steps were applied. Current amplitude was increased in 15 pA steps until at least 1.5 times rheobase, the level at which the characterization of the firing pattern was made. Only cells exhibiting clear FS (including stuttering cells) and adapting electrical types were included in the analysis.

NEUROSCIENCE

STATISTICS

Dynamic Gain Calculation. Population frequency-response characterization was restricted to layer 2/3 prefrontal FS and AD interneurons and was assessed as previously described (11, 12). This analysis aims to achieve an in vivo-like operating point, mimicking a situation in which a high rate of synaptic inputs provides a continuously changing net background current and a neurons' firing is driven not by the average input but by its transient depolarizing excursions (17). Fluctuating current inputs were synthesized as Ornstein-Uhlenbeck noises x(t) with either 5 or 25 ms correlation time. These values were chosen to approximate the case of uncorrelated inputs filtered through the synaptic currents' decay time constants (5 ms) or the case of slow temporal correlations in the input due to correlated network activity (25 ms). Inputs' SD was adjusted to obtain similar firing rates (around 4 Hz) and coefficients of variation of the interspike intervals (around 1) for both correlation times. Neurons were first depolarized to -60 mV with constant current, and different realizations of the fluctuating noise were injected in 30-s-long episodes, separated by 15-s-long resting, for as long as the recording did not display signs of deterioration, such as baseline drifts or spike overshooting to positive voltages less than 20 mV. For experiments presented in Fig. 3, a theta power enhanced stimulus was created by adding a 4 to 12 Hz bandpass filtered white noise to the 5 ms input. The SD of the bandpass filtered signal was normalized to two times the SD of the 5 ms signal. The amplitude of the combined signal was reduced until the firing rate was again close to the 5 Hz target rate. APs were detected as 0 mV crossings on the voltage trace, and the AP times were annotated. From these, a spike-triggered average (STA) input current was obtained by summing up 1-s-long stimulus segments centered on the AP times for all cells of a given condition and dividing by the total number of APs.

The complex dynamic gain function G(f) was calculated as the ratio of the complex conjugate of the Fourier transform of the STA, F(STA₁)*, and the Fourier transform of the autocorrelation of the stimulus:

$$G(f) = \frac{F(STA_I)^*}{F(AC_I)},$$

where $AC_I(\tau) = \langle x(t)x(t+\tau)\rangle$, and τ denotes the time lag. In this frequency domain equation, a frequency component in the numerator is divided by a component of the same frequency in the denominator. When a sine signal $I_{sin} = A_{sin} \cdot sin 2\pi f_{sin} t$ is modulated onto the current, it causes a contribution A_{sin}^2 to $F(AC_i)$ exactly at the frequency f_{sin} (SI Appendix, Fig. S1B). It will also cause each AP to occur slightly earlier or later, depending on the voltage modulation induced by I_{\sin} at the AP time. This leads to a sinusoidal modulation of the firing rate and therefore to a larger contribution of the frequency component to the STA, (SI Appendix, Fig. S1A). This method of sinusoidal modulation to calculate the dynamic gain leads to the same results if the sine current amplitude is sufficiently large to dominate over the frequency component in the Ornstein-Uhlenbeck noise but also sufficiently small to avoid nonlinear modulation, characterized, for instance, by a change in the coefficient of variation of the interspike interval distribution. The dynamic gain at the sine frequency can be calculated as $G(f) = \frac{2}{A_{in}} \cdot \frac{1}{N} \cdot \sum_{k=1}^{N} e^{-i2\pi f_{in}t_k}$ with the N AP times t_k .

In previous experiments, the dynamic gain values we obtained with those two methods were very similar (28); see also *SI Appendix*, Fig. S1.

In order to improve signal-to-noise ratio, G(f) was filtered in the frequency domain by a Gaussian filter w(f') centered at frequency f'=f and a frequency-dependent window size with SD of $f/2\pi$:

$$w(f') = \frac{1}{\sqrt{2\pi} \left(\frac{f}{2\pi}\right)} exp \left[\frac{-1}{2} \left(\frac{f'-f}{f/2\pi}\right)^2 \right].$$

The filtered dynamic gain function $G_w(f)$ thus becomes

$$G_{w}(f) = rac{\int G(f') \cdot w(f') \cdot df'}{\int w(f') \cdot df'}.$$

The magnitude and phase of this filtered, complex dynamic gain function are reported in Figs. 2–4

For the dynamic gains reported in Fig. 2, the data comprise the following: for AD neurons, 19,563 spikes from 12 cells and 20,427 spikes from 10 cells (5 and 25 ms, respectively) and, for FS neurons, 9,792 spikes from 7 cells and 15,023 spikes from 9 cells (5 and 25 ms, respectively). Five of the 10 AD neurons tested with 5 ms correlated stimuli were also tested with the theta-supplemented 5 ms input. In addition to these, another 5 were used to obtain the gains in Fig. 3 (14,847 spikes, for 5 ms stimulus and 18,067 spikes for theta-supplemented 5 ms stimulus). Cls were obtained by bootstrap resampling. Two thousand bootstrapped gain curves were calculated from the same number of STAs obtained by randomly sampling from all APs used in the population gain calculation. The Cls are defined by the percentiles 2.5 and 97.5 at each frequency point in the 2,000 gain curves. The distribution of this bootstrap statistic was not different from normal (Kolmogorov-Smirnov test). To

- G. Buzsáki, A. Draguhn, Neuronal oscillations in cortical networks. Science 304, 1926–1929 (2004)
- J. Cannon et al., Neurosystems: Brain rhythms and cognitive processing. Eur. J. Neurosci. 39, 705–719 (2014).
- 3. J. E. Lisman, O. Jensen, The θ - γ neural code. Neuron 77, 1002–1016 (2013).
- J. A. Cardin et al., Driving fast-spiking cells induces gamma rhythm and controls sensory responses. Nature 459, 663–667 (2009).
- M. A. Whittington, R. D. Traub, J. G. Jefferys, Synchronized oscillations in interneuron networks driven by metabotropic glutamate receptor activation. *Nature* 373, 612–615 (1995)
- F. G. Pike et al., Distinct frequency preferences of different types of rat hippocampal neurones in response to oscillatory input currents. J. Physiol. 529, 205–213 (2000).
- J. Veit, R. Hakim, M. P. Jadi, T. J. Sejnowski, H. Adesnik, Cortical gamma band synchronization through somatostatin interneurons. *Nat. Neurosci.* 20, 951–959 (2017).
- R. Hakim, K. Shamardani, H. Adesnik, A neural circuit for gamma-band coherence across the retinotopic map in mouse visual cortex. eLife 7, e28569 (2018).
- G. Chen et al., Distinct inhibitory circuits orchestrate cortical beta and gamma band oscillations. Neuron 96, 1403–1418.e6 (2017).
- H. Köndgen et al., The dynamical response properties of neocortical neurons to temporally modulated noisy inputs in vitro. Cereb. Cortex 18, 2086–2097 (2008).
 E. Lazarov et al., An axon initial segment is required for temporal precision in action
- potential encoding by neuronal populations. *Sci. Adv.* **4**, eaau8621 (2018).

 12. M. H. Higgs, W. J. Spain. Conditional bursting enhances resonant firing in neocortical
- layer 2-3 pyramidal neurons. *J. Neurosci.* **29**, 1285–1299 (2009).

 13. N. Brunel, F. S. Chance, N. Fourcaud, L. F. Abbott, Effects of synaptic noise and filtering
- on the frequency response of spiking neurons. *Phys. Rev. Lett.* **86**, 2186–2189 (2001).

 14. B. Naundorf, F. Wolf, M. Volgushev, Unique features of action potential initiation in
- cortical neurons. *Nature* **440**, 1060–1063 (2006).

 15. J. F. A. Poulet, S. Crochet, The cortical states of wakefulness. *Front. Syst. Neurosci.* **12**, 64 (2019).
- D. Feldmeyer, G. Qi, V. Emmenegger, J. F. Staiger, Inhibitory interneurons and their circuit motifs in the many layers of the barrel cortex. Neuroscience 368, 132–151 (2018).

identify the portions of the gain curves that are significantly different from zero, we calculated a noise floor. It was calculated by cyclically shifting original spike times by a random time interval, larger than 5 correlation times, and calculating 2,000 "random time-triggered averages," which were used to calculate "gain curves." The noise floor was defined as the 95th percentile of these "gain curves." The gain curves in Figs. 2–4 were displayed either until they were crossed by the noise floor or up to 1,000 Hz, if noise floor crossing happened at a frequency > 1,000 Hz.

Hilbert Analysis. The stimulus's theta phase component was extracted by filtering with an infinite impulse response bandpass filter with 6 pole Butterworth characteristics. The filter was designed in Igor Pro-8 with pass-band limits of 3.5 and 10.5 Hz for the sample frequency of 100 kHz. Used twice, once in forward time, once in reversed time, the filter results in zero-delay filtering of the input. Fourier analysis of the input and output shows effective isolation of the 4 to 12 Hz component. The phase and amplitude of this component were obtained by conventional Hilbert analysis. APs were stratified according to the phase of the theta component at the AP time to perform the analysis in Fig. 4.

Statistics. Paired samples, two-sided Wilcoxon rank tests were performed to test the single neuron data in Figs. 3 and 4. W-statistics and *P* values are given in figures and legends. The *P* values in Fig. 4*D* are not corrected for the dual comparison.

Data Availability. Data are available from the Max Planck Digital Library at https://edmond.mpdl.mpg.de/imeji/collection/pdxNFpq JurbDDeop (29). The code, written in Igor Pro-8 and 9, used to analyze raw data and generate the dynamic gain curves, is included in the data repository. The code is continuously maintained. The latest version is available in GitHub at https://github.com/Apneef/AnTools

ACKNOWLEDGMENTS. This work is supported by Bundesministerium für Bildung und Forschung (BMBF; Federal Ministry of Education and Research) Grant 01GQ1005B (to F.W., A.N.); BMBF (Federal Ministry of Education and Research) Grant 01GQ1005E (to F.W.); Deutsche Forschungsgemeinschaft (German Research Foundation) 436260547, in relation to NeuroNex (National Science Foundation 2015276) (to J.F.S., F.W., A.N.); Volkswagen Foundation Grant ZN2632 (to F.W.); GGNB Excellence Stipend of the University of Göttingen (to R.M.M.); and the Max Planck Society.

- A. Destexhe, M. Rudolph, D. Paré, The high-conductance state of neocortical neurons in vivo. Nat. Rev. Neurosci. 4, 739–751 (2003).
- A. Adhikari, M. A. Topiwala, J. A. Gordon, Synchronized activity between the ventral hippocampus and the medial prefrontal cortex during anxiety. *Neuron* 65, 257–269 (2010).
- R. T. Canolty, R. T. Knight, The functional role of cross-frequency coupling. Trends Cogn. Sci. 14, 506–515 (2010).
- N. Brunel, V. Hakim, Fast global oscillations in networks of integrate-and-fire neurons with low firing rates. Neural Comput. 11, 1621–1671 (1999).
- C. Geisler, N. Brunel, X. J. Wang, Contributions of intrinsic membrane dynamics to fast network oscillations with irregular neuronal discharges. *J. Neurophysiol.* 94, 4344–4361 (2005).
- T. Tchumatchenko, A. Malyshev, F. Wolf, M. Volgushev, Ultrafast population encoding by cortical neurons. J. Neurosci. 31, 12171–12179 (2011).
- H. R. Joo, L. M. Frank, The hippocampal sharp wave-ripple in memory retrieval for immediate use and consolidation. *Nat. Rev. Neurosci.* 19, 744–757 (2018).
- T. Klausberger, P. Somogyi, Neuronal diversity and temporal dynamics: The unity of hippocampal circuit operations. Science 321, 53–57 (2008).
- C. Scheffzük et al., Selective coupling between theta phase and neocortical fast gamma oscillations during REM-sleep in mice. PLoS One 6, e28489 (2011).
- J. Doose, G. Doron, M. Brecht, B. Lindner, Noisy juxtacellular stimulation in vivo leads to reliable spiking and reveals high-frequency coding in single neurons. *J. Neurosci.* 36, 11120–11132 (2016).
- A. H. Meyer, I. Katona, M. Blatow, A. Rozov, H. Monyer, In vivo labeling of parvalbumin-positive interneurons and analysis of electrical coupling in identified neurons. J. Neurosci. 22, 7055–7064 (2002).
- O. Revah et al., Dynamic gain analysis reveals encoding deficiencies in cortical neurons that recover from hypoxia-induced spreading depolarizations. J. Neurosci. 39, 7790–7800 (2019).
- A. Neef, Flexible interneuron function. Edmond. https://doi.org/10.17617/3.8e. Deposited 16 December 2019.